Coupling and electrical control of structural, orbital and magnetic orders in perovskites

Julien Varignon[a],[1,†] Nicholas C. Bristowe,[1,2,†] Eric Bousquet,[1] and Philippe Ghosez[1]

[1]*Physique Théorique des Matériaux, Université de Liège (B5), B-4000 Liège, Belgium*[‡]
[2]*Department of Materials, Imperial College London, London SW7 2AZ, UK*

(Dated: August 20, 2015)

Perovskite oxides are already widely used in industry and have huge potential for novel device applications thanks to the rich physical behaviour displayed in these materials. The key to the functional electronic properties exhibited by perovskites is often the so-called Jahn-Teller distortion. For applications, an electrical control of the Jahn-Teller distortions, which is so far out of reach, would therefore be highly desirable. Based on universal symmetry arguments, we determine new lattice mode couplings that can provide exactly this paradigm, and exemplify the effect from first-principles calculations. The proposed mechanism is completely general, however for illustrative purposes, we demonstrate the concept on vanadium based perovskites where we reveal an unprecedented orbital ordering and Jahn-Teller induced ferroelectricity. Thanks to the intimate coupling between Jahn-Teller distortions and electronic degrees of freedom, the electric field control of Jahn-Teller distortions is of general relevance and may find broad interest in various functional devices.

[a] corresponding author: julien.varignon@ulg.ac.be

INTRODUCTION

Widespread interest in transition metal perovskite-like oxides over the last several decades can be ascribed to two key discoveries: high-temperature superconductivity in the cuprates and colossal magnetoresistance in the manganites [1, 2]. Physical behavior exhibited by perovskites is by no means limited to these two phenomena, but also includes ferroelectricity and (anti)ferromagnetism or both simultaneously and coupled in magnetoelectric multiferroics, metal-insulator transitions and thermoelectricity, to name a few. The wide range of functional properties is usually thanks to an interplay between the structural (lattice), electronic (orbital and charge) and magnetic (spin) degrees of freedom allowed within the transition metal oxides [3–6]. This playground for novel materials physics is not only of fundamental academic interest, but oxide perovskites have already entered industry and have huge potential for novel device applications [7, 8].

The possibility of tuning the magnetic properties of a material with an applied electric field has received particular attention for low energy consumption spintronic devices [7, 9]. In this regard, a promising route to achieve ferroelectricity in magnets is *via* so-called the hybrid improper ferroelectricity [10–12]. Here, non-polar modes such as antiferrodistortive (AFD) motions, which are ubiquitous in perovskites, eventually combined with antipolar motions, simultaneously drives the polarization and can couple to the magnetic orders [13–17]. However, those motions are rather weakly linked to the electronic properties and hence the magnetoelectric coupling is likely not the most efficient. It would be advantageous to replace the AFD or anti-polar motions by another lattice distortion which couples directly to the electronic properties. Such a motion common in perovskites is the Jahn-Teller distortion (JT), and recently, a hybrid improper ferroelectricity mechanism involving such a distortion was reported in metal-organic frameworks [18, 19], yielding promising magnetoelectric multiferroic properties.

In an attempt to generalize and extend the concept to any perovskite, we reveal from a universal symmetry analysis that a hybrid improper polarization may arise solely from Jahn-Teller distortions. This mechanism is intrinsic to the perovskite structure and demonstrated here on the vanadate perovskites which exhibit a complex structural ground state including different Jahn-Teller distortions. Using first-principles calculations, we reveal in $AA'V_2O_6$ superlattices an unprecedented orbital ordering and purely Jahn-Teller induced ferroelectricity. We demonstrate that this enables an electric field control of both JT distortions and magnetism. Since JT distortions are intimately connected to electronic degrees of freedom [20], such as magnetism, orbital orderings and metal-insulator phase transitions to name a few, the proposed mechanism may find broader interest for novel functional devices outside the field of magnetoelectrics.

BULK $A^{3+}V^{3+}O_3$

Whilst the V^{4+} perovskites (e.g. $SrVO_3$ [21]) have been studied mainly for their interesting metallic properties, the V^{3+} perovskites are Mott insulators. $A^{3+}V^{3+}O_3$ compounds have attracted much attention since the fifties when they were first synthesized[22]. During this time, many studies began to determine their magnetic, electronic and structural properties [23–39]. A central theme at the core of these properties in vanadates is the so-called Jahn-Teller (JT) distortion. The famous Jahn-Teller theorem claims that a material with degenerate electronic states will be unstable towards undergoing a structural distortion lowering its symmetry to remove the electronic degeneracy. In other words, the Jahn-Teller effect is an electronic instability that can cause a structural and metal-insulator phase transition. For instance, in the cubic perovskite symmetry, the crystal field effect splits the d electron levels into a lower lying degenerate three-fold t_{2g} and a higher lying degenerate two-fold e_g state. Hence in $3d^2$ systems such as the rare-earth vanadates, a Jahn-Teller distortion is required to split the t_{2g} levels in order to form a Mott insulating state. We note here the distinction between the Jahn-Teller effect and what we call the Jahn-Teller distortion in this study. Here we define the Jahn-Teller distortion by the symmetry of the atomic distortion as shown in Figure 1.b and Figure 1.d. Whilst a distortion of this symmetry will by definition remove the d electronic degeneracy, the origin of such a distortion does not necessarily need to appear from the Jahn-Teller effect. An important result of this study is that the Jahn-Teller distortion can instead be induced by structural anharmonic couplings, being therefore not only restricted to Jahn-Teller active systems [40].

In the vanadates, two different JT distortions are observed [24–26, 33], with each one consisting to two V-O bond length contractions and two elongations, often labelled as a Q_2 distortion [42]. The corresponding distortions are displayed in Figure 1 where they are compared to the antiferrodistortive (AFD) motions. The AFD motions can be viewed as oxygen octahedra rotations around an axis going through the B cations, while the Jahn-Teller distortions in the present case correspond to oxygen rotations around an axis going through the A cations. Both JT and AFD motions can be either in-phase (Figure 1.a+b) or anti-phase (Figure 1.c+d) between consecutive layers and therefore appear at the M or R points of the Brillouin zone respectively. Consequently, we label the Jahn-Teller distortions as Q_2^+ (M_3^+
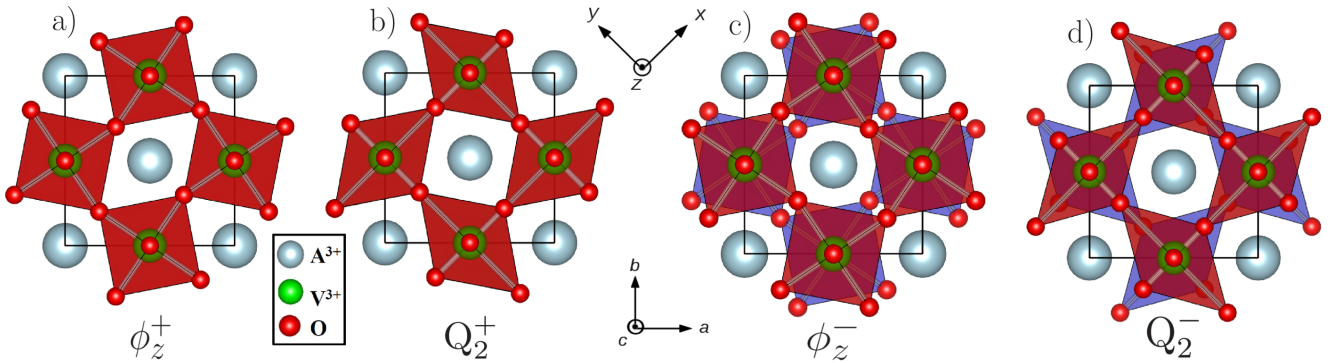
FIG. 1. Comparison of JT and AFD motions around the z axis; a) in-phase ϕ_z^+ AFD motion (M_2^+ mode); b) in-phase Q_2^+ Jahn-Teller motion (M_3^+ mode); c) anti-phase ϕ_z^- motion (R_5^- mode); d) anti-phase Q_2^- motion (R_3^- mode). Octahedras for the plane in $z=0$ are plotted in red and in blue for the plane in $z=c/2$. The AFD motions can also appear around the y and z axes (not shown), whereas the Jahn-Teller motions only manifest around the z axis in the vanadates.

mode) and Q_2^- (R_3^- mode). While AFD motions do not distort the BO_6 octahedra, JT motions lift the degeneracy of the d levels through octahedra deformations. According to such distortions, the V^{3+} $3d^2$ occupation consists of either a d_{xy} and d_{xz} t_{2g}^2 or a d_{xy} and d_{yz} t_{2g}^2 state in an ideal picture. Nearest-neighbor vanadium sites within the (xy)-plane develop opposite distortions and hence alternative d_{xy} and d_{xz} / d_{xy} and d_{yz} occupations as shown in the top panel of Figure 2. Along the $\vec{c}$ axis, the octahedra deformations and hence orbital ordering are either in phase (C-type orbital order) or anti-phase (G-type orbital order) for the Q_2^+ or Q_2^- Jahn-Teller distortion respectively (see Figure 2 bottom panel). Crucially, the orbital ordering determines the magnetic ordering through superexchange interactions [43–45]. Strongly overlapping and parallel orbitals between neighboring sites favors antiferromagnetic superexchange interactions. With this in mind, the Q_2^+ motion favors a purely antiferromagnetic solution called G-AFM whilst the Q_2^- motion favors (xy)-plane antiferromagnetic alignment and ferromagnetic out-of-plane alignment called C-AFM. In other words, a C-type orbital ordering (C-o.o.) is linked to a G-type antiferromagnetic ordering (G-AFM), while a G-type orbital ordering (G-o.o.) is linked to a C-type antiferromagnetic ordering (C-AFM). Experiments indeed observe both G-AFM and C-AFM magnetic phases in the vanadates, with each magnetic ordering favoring a certain structural symmetry [25, 26, 33].

At room temperature, all rare-earth $A^{3+}V^{3+}O_3$ vanadates crystallize in a *Pbnm* structure [24–26, 33]. With decreasing temperature, they undergo an orbital ordering phase transition to a G-type orbital ordered (G-o.o.) phase between 200K and 150K (depending on the A-cation size). This transition is accompanied by a symmetry lowering from *Pbnm* to $P2_1/b$. A magnetic phase transition from a paramagnetic to an C-AFM antiferromagnetic state occurs within this phase at a slightly lower temperature between 150K and 100K. Finally, for the smallest A cations (A=Yb-Dy, Y), another orbital ordering phase transition to a purely C-type (C-o.o.) arises and is accompanied by a structural phase transition from $P2_1/b$ back to *Pbnm*, and a magnetic phase transition from C-AFM to G-AFM. For medium A cations (A=Tb-Nd), a coexistence of $P2_1/b$ (G-oo) and *Pbnm* (C-oo) phases is reported [26, 46]. No further transitions are found for larger A cations (A=Pr, Ce and La).

To better understand the distorted structures of vanadates, we perform a symmetry mode analysis [47, 48] of the allowed distortions with respect to a hypothetical cubic phase on three different compounds, covering a wide range of A-cation sizes: YVO_3, $PrVO_3$ and $LaVO_3$. The analysis is performed on experimental structural data, and the amplitudes of distortions are summarized in Table I.

In the *Pbnm* phase ($a^-a^-c^+$ in Glazer's notations [51]), all three vanadates develop two unique antiferrodistortive (AFD) motions ϕ_{xy}^- ($\phi_{xy}^-=\phi_x^-+\phi_y^-$, $a^-a^-c^0$) and ϕ_z^+ ($a^0a^0c^+$). Table I shows that the magnitudes of these AFD motions strengthen with decreasing A-cation size as expected *via* simple steric arguments [52]. Within this *Pbnm* tilt pattern, the Q_2^+ lattice motion is already compatible and does not require any symmetry lowering to appear [38]. This latter observation is in agreement with the sizeable Q_2^+ lattice distortion extracted from our analysis on room temperature structures, despite the fact that no orbital-ordering has yet been reported for this temperature range [25, 26]. The *Pbnm* phase then appears to always be a pure Q_2^+ phase. Additionally, an anti-polar X_5^- mode whose motion is in the (xy)-plane is allowed in the *Pbnm* symmetry (see supplementary materials).

Going to the $P2_1/b$ symmetry, a subgroup of *Pbnm*, the aforementioned AFD motions are still present, but the Q_2^- distortion is now allowed and would lead to a G-o.o. phase. However, the $P2_1/b$ phase is never an exclusive Q_2^- phase
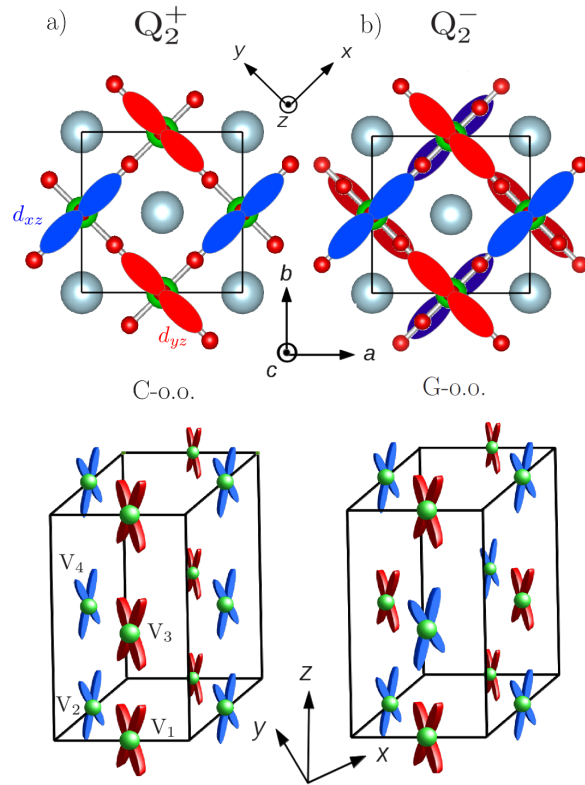
FIG. 2. Schematic picture of the idealized orbital orderings between the d_{xz} (blue) and d_{yz} (red) orbitals. The d_{xy} orbital is not shown for clarity. a) Top view of the orbital-ordering induced by a Q_2^+ distortion (top). Consecutive planes exhibit identical orbital orderings labelled as a C-type orbital-ordering (C-o.o.) (middle). This results in a G-AFM ordering. b) Orbital-ordering induced by a Q_2^- distortion (top). Consecutive planes exhibit out-of phase orbital orderings labelled as a G-type orbital-ordering (G-o.o.) (middle). This results in a C-AFM ordering.

but always coexists with the Q_2^+ distortion, even for the larger A cations (A=Pr, La). A mixed C-o.o. and G-o.o. should then manifest for all $P2_1/b$ structures, independent orthorhombic/monoclinic phase coexistence. Additionally, another anti-polar X_3^- mode, whose motion is now along the z direction, arises in this new phase (see supplementary materials).

In order to understand the origin and coupling between these distortions, we can perform a free energy $\mathcal{F}$ expansion (see methods) around a hypothetical cubic $Pm\bar{3}m$ phase with respect to the different distortions. Among all the possible terms in the $Pbnm$ phase, two trilinear couplings are identified:

$$\mathcal{F}_{tri,\,Pbnm} \propto \phi_{xy}^-\,\phi_z^+\,X_5^- \;+\; \phi_{xy}^-\,X_5^-\,Q_2^+ \tag{1}$$

Within the $Pbnm$ symmetry, when ϕ_{xy}^- and ϕ_z^+ are non zero in magnitude, the free energy of the system is automatically lowered by the appearance of X_5^- due to the first trilinear term of Equation 1. Similarly, through the appearance of X_5^-, the free energy is again lowered by forcing the appearance of the Q_2^+ motion thanks to the second trilinear coupling. This explains the presence of the Q_2^+ distortion in the $Pbnm$ phase of vanadates, even at room temperature. This demonstrates that, in addition to its possible appearance as an electronic instability, it may also appear as a structural anharmonic improper mode within the $Pbnm$ phase (whose strength depends on the coupling constant) even in non Jahn-Teller active materials [40, 41]. Going to the $P2_1/b$ phase, two additional trilinear couplings are identified:

$$\begin{aligned}\mathcal{F}_{tri,\,P2_1/b} &\propto \phi_{xy}^-\,\phi_z^+\,X_5^- \;+\; \phi_{xy}^-\,X_5^-\,Q_2^+ \\ &+ Q_2^+\,Q_2^-\,X_3^- \;+\; \phi_z^+\,X_3^-\,\phi_z^-\end{aligned} \tag{2}$$

The orbital-ordering phase transition to a G-o.o. phase experimentally observed between 150K and 200K for all vanadates [25, 26] manifests itself through the appearance of a Q_2^- distortion. Consequently, through the third

trilinear coupling of Equation (2), both JT distortions produce the additional anti polar X_3^- motion . This is in agreement with the experimental data of table I. Finally, an extra ϕ_z^- $(a^0a^0c^-)$ AFD motion arises in the $P2_1/b$ phase through the last trilinear coupling, yielding a rare $a^-a^-c^\pm$ tilt pattern with both in-phase and out-of phase AFD motion around the $\vec{c}$ axis. This tilt pattern has previously been predicted to appear within this space group [38].

Therefore, within this $P2_1/b$ phase, both Jahn-Teller distortions coexist, but likely with different origins. The Q_2^+ mode is "pinned" into the system through an improper anharmonic coupling with the robust AFD motions while the Q_2^- mode may appear through the traditional Jahn-Teller electronic instability. It is interesting to note that this coexistence is allowed due to the improper appearance of Q_2^+, despite there likely being a competition between both JTs. This competition would be understood as an electronic origin to favor one type of orbital ordering over the other, producing a biquadratic coupling with a positive coefficient in the free energy expansion. In the light of there being an abundance of Q_2^+ with respect to Q_2^- phases across the perovskites, we then propose whether it is this improper appearance of Q_2^+ *via* the robust AFD motions that helps favor this phase universally. The vanadates would then be a special case where the Q_2^- instability is robust enough to appear despite this competition. This universal symmetry analysis and free energy expansion rationalize the origin of the coexisting orbital ordered phase in the $P2_1/b$ symmetry as observed in vanadates both experimentally and theoretically [25, 26, 37, 38].

The coexistence of both Jahn-Teller motions in the vanadates, will also clearly affect the orbital ordering and consequently the magnetic ordering. One might expect a complex canted magnetic ordering to occur, resembling partly C-AFM and partly G-AFM, as indicated experimentally from neutron scattering on several vanadates. While a pure G-type AFM ordering is observed in the $Pbnm$ phase of YVO$_3$ with magnetic moments lying along the $\vec{c}$ axis, a non-collinear spin arrangement is observed in the $P2_1/b$ phase [29, 30, 49, 53]. Indeed, the spin arrangement corresponds to a C-AFM ordering with magnetic moments located in the (ab)-plane plus a weaker G-AFM ordering with magnetic moments along the $\vec{c}$ axis. This observation is totally in line with the coexistence of both Jahn-Teller distortions in the $P2_1/b$ phase. Indeed, while the $Pbnm$ phase can only stabilize a C-o.o./G-AFM ordering, the $P2_1/b$ phase has a dominant G-o.o./C-AFM character coexisting with a smaller C-o.o. and consequently a weak G-AFM ordering may appear with magnetic moments along the $\vec{c}$ axis [53]. Interestingly, even at the collinear level, our first-principles calculations on the three aforementioned bulk vanadates already indicate this complex magnetic ordering in the $P2_1/b$ phase. Within the YVO$_3$ $Pbnm$ G-AFM C-o.o. ground state, all magnetic sites hold roughly the same magnetic moment ($1.811 \pm 0.002~\mu_B$) indicating a purely C-o.o./G-AFM ordering as observed experimentally. Going to the $P2_1/b$ G-o.o./C-AFM phase of both PrVO$_3$ and LaVO$_3$, two magnetic sublattices are observed. Indeed, two different magnitudes for the magnetic moments are found in consecutive (xy)-VO$_2$ layers (1.833 ± 0.001 and 1.826 ± 0.001 for PrVO$_3$ and $1.822 \pm 0.002~\mu_B$ and $1.813 \pm 0.001~\mu_B$ for LaVO$_3$) which can be seen as a dominant G-o.o. plus a smaller C-o.o. on the top of the latter one, and consequently a dominant C-AFM plus a weaker G-AFM.

$(AVO_3)_1/(A'VO_3)_1$ LAYERED STRUCTURES

Magneto-electric multiferroics are widely studied due to their intriguing coupling between ferroelectricity and magnetism (electric field control of magnetism and conversely), and are proposed as promising candidates for lower energy consumption spintronic devices [7, 9]. However, materials combining both ferroelectric and (anti)-ferromagnetic order parameters are elusive in nature and the identification of new single phase multiferroics remains a challenge for modern day research [54].

Hybrid improper ferroelectricity, in which a polar distortion is driven by two non-polar motions, emerged recently as a possible new mechanism to induce ferroelectricity in otherwise non-ferroelectric compounds [10–13]. When considering magnetic compounds, the trilinear coupling between polar and non-polar lattice distortions achieved in such systems appeared moreover as a promising pathway to achieve enhanced magneto-electric coupling [13, 14, 18, 19, 55]. Rondinelli and Fennie clarified [12] the emergence of rotationally driven ferroelectricity in ABO$_3$/A'BO$_3$ superlattices, providing concrete rules for the design of new hybrid improper ferroelectrics.

Following the same spirit, we consider $(AVO_3)_1/(A'VO_3)_1$ structures with planes of different A cations layered along the [001] direction. This structure can either appear naturally as in the double perovskites, or through single layer precision epitaxial deposition techniques. The free energy expansion around a $P4/mmm$ layered reference structure (equivalent to $Pm\bar{3}m$ in bulk) then becomes:

$$\mathcal{F}_{tri,Pb} \propto \phi_{xy}^-\,\phi_z^+\,P_{xy} \;+\; \phi_{xy}^-\,P_{xy}\,Q_2^+$$
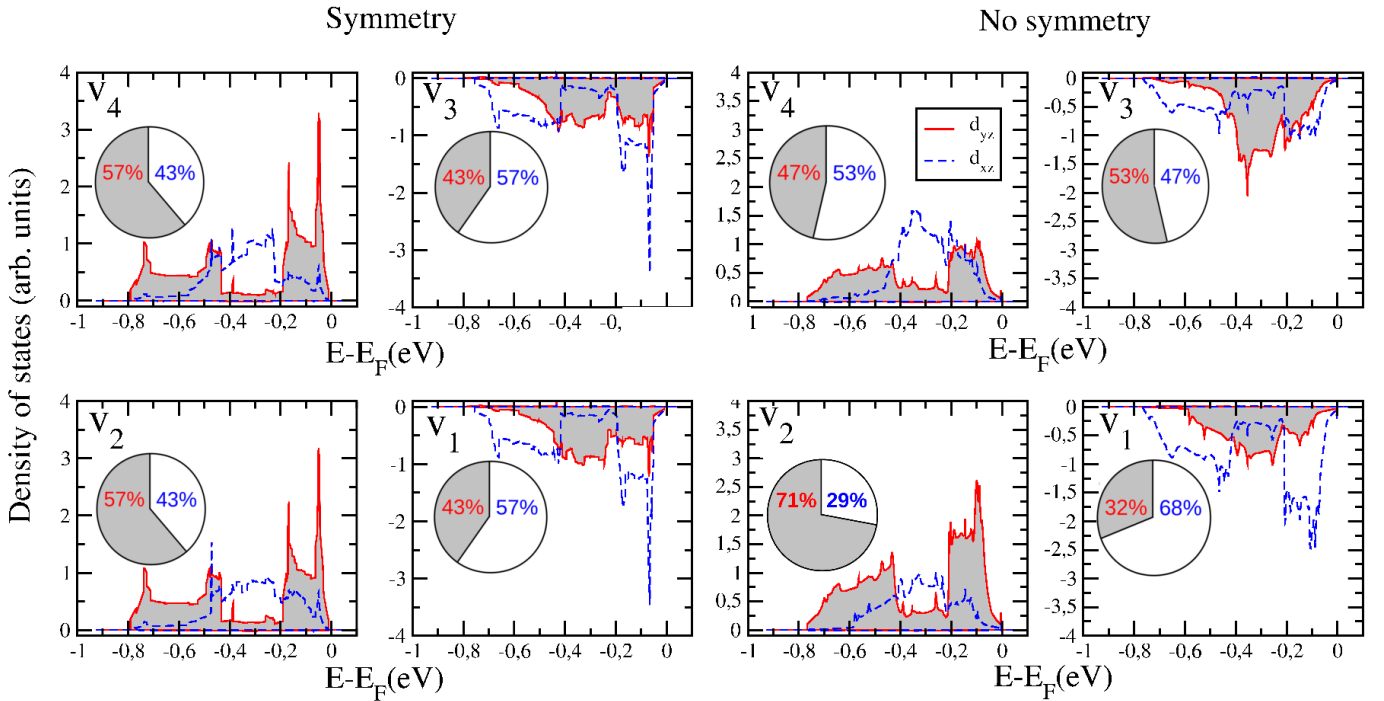$$+\; Q_2^+\,Q_2^-\,P_z \;+\; \phi_z^+\,P_z\,\phi_z^- \tag{3}$$

FIG. 3. Projected density of states on the d_{yz} (grey filled red curve) and d_{xz} (unfilled blue dashed curve) orbitals of vanadium by imposing the $Pb2_1m$ atomic positions and computing the energy with $Pb2_1m$ symmetry (left) for the electronic wavefunction and by removing the symmetry (right) for the electronic wavefunction. d_{xy} is not displayed for clarity. V_1 (V_3) and V_2 (V_4) are located within the same (001) plane as defined in Figure 2. The percentage of total d_{yz} (red) and d_{xz} (blue) character on each vanadium is shown as a pie chart to illustrate the change from C-o.o to C+G-o.o. once the symmetry constraint for the wavefunction is lifted.

The first observation is that the symmetry breaking due to the A cation layering turns the X antipolar modes to polar modes, i.e. in-plane (110) P_{xy} and out-of-plane (001) P_z [10, 12, 54, 56, 57]. The first and fourth trilinear couplings of Equation 3 correspond to the rotationally driven hybrid improper ferroelectricity mechanism [10–12]. The second trilinear term links the in-plane polarization to both an antiferrodistortive (AFD) and Jahn-Teller (JT) distortion, already observed in reference 18. However, we identify in Eq. 3 a new trilinear term $Q_2^+ Q_2^- P_z$ coupling the out-of-plane polarization P_z to both JT distortions. Since JT distortions are intimately connected to orbital-orderings and particular magnetic states as discussed in the previous section , we can expect to have a direct and strong coupling between polarization and magnetism from this term.

In the present work, we have performed first-principles calculations in order to show that $(AVO_3)_1/(A'VO_3)_1$ layered structures are indeed ferroelectric and develop both in plane and out-of-plane polarizations. On the one hand, P_{xy} appears as a slave to the rotations and is indirectly linked to magnetism through the modification of the superexchange path as in the usual rotationally driven ferroelectrics [13]. On the other hand, P_z appears thanks to an electronic instability manifested as a particular orbital and magnetic ordering. Finally, we demonstrate that an electric control of the magnetic state is indeed possible, providing a novel paradigm for the elusive magnetoelectric multiferroics.

In order to test the above hypothesis, we considered two different superlattices: $(PrVO_3)_1/(LaVO_3)_1$ (PLVO) and $(YVO_3)_1/(LaVO_3)_1$ (YLVO). First principles geometry relaxations (see method section) of the superlattices converged to two metastable states: a C-AFM ordering is found in a Pb structure (equivalent to the $P2_1/b$ in bulk) while a G-AFM ordering is found in a $Pb2_1m$ symmetry (equivalent to $Pbnm$ in bulk). We find that PLVO adopts a Pb C-AFM ground state while YLVO adopts a $Pb2_1m$ G-AFM ground state. The symmetry adapted modes and computed polarizations of all metastable phases are presented in the supplementary material. As predicted, the $Pb2_1m$ ground state of YLVO only exhibits a P_{xy} polarization, whose magnitude is 7.89 $\mu C.cm^{-2}$. However, the Pb ground state of PLVO develops both P_{xy} and P_z polarizations of 2.94 and 0.34 $\mu C.cm^{-2}$ respectively. The P_z contribution indicates a Jahn-Teller induced ferroelectricity (third term of Equation 3). Below we explore the origin of P_{xy} and P_z in more detail.

Bulk vanadates exhibit a $Pbnm$ phase at room temperature and hence both superlattices should first go to the equivalent $Pb2_1m$ intermediate phase. We therefore begin by providing insight on the driving force yielding the
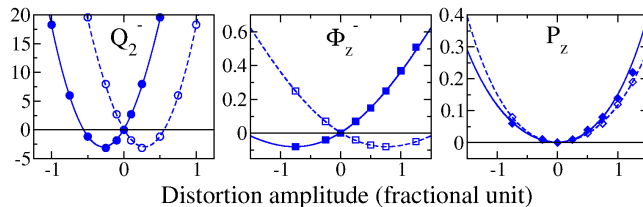
FIG. 4. Energy gains (in meV) by condensing various amplitudes of the individual Q_2^-, ϕ_z^- and P_z distortions. Potentials are plotted for a '↑' (open blue symbols) and a '↓' (filled blue symbols) initial electronic polarization.

various distortions within this phase. For this purpose, we condense different amplitudes of distortions (see methods) within the metastable $Pb2_1m$ state of the PLVO superlattice starting from an ideal $P4/mmm$ structure (for each potential, see supporting information). Four main distortions are then present in this $Pb2_1m$ phase: ϕ_{xy}^-, ϕ_z^+, Q_2^+ and P_{xy}. As expected, the two antiferrodistortive motions are strongly unstable (approximately 1 eV of energy gains for each) and are the primary order parameters of this $Pb2_1m$ symmetry. P_{xy} and Q_2^+ present single wells which are the signature of an improper anharmonic appearance [55]. Therefore, the P_{xy} polarization appears through a hybrid improper mechanism driven by the two rotations through the first term of Equation 3. Furthermore, as predicted in the first section, this analysis suggests that the Q_2^+ appears with a structural hybrid improper mechanism rather than an electronic instability in this compound.

Having considered the intermediate $Pb2_1m$ phase, we next turn our attention to the phase transition of PLVO to its Pb ground state. Curiously, a phonon calculation on the intermediate $Pb2_1m$ phase did not identify any unstable modes, indicating that no lattice motions can be responsible for the phase transition. Clearly, the system has to switch from G-AFM to C-AFM and therefore in an attempt to understand this phase transition we performed the following two sets of calculations. The atomic positions were fixed to the intermediate $Pb2_1m$ structure and the energy was computed i) with imposed and ii) with no imposed, $Pb2_1m$ symmetry for the electronic wavefunction, both within the two possible magnetic states. While for the G-AFM calculations, no energy difference is observed between calculations with and without symmetry, the C-AFM calculation with no symmetry leads to a lower energy (around 4.5 meV) than the one with imposed symmetry. The only difference between the two calculations is that the electronic structure is allowed to distort and consequently breaks the symmetry. We discover that, even with the atoms fixed in centrosymmetric positions along the z axis, the electronic instability creates an out-of-plane polarization P_z of 0.04 $\mu C.cm^{-2}$.

In order to understand the nature of this electronic instability, we plot the projected density of states on vanadiums in Figure 3. Starting from the projected density of states with $Pb2_1m$ symmetry, consecutive atoms along the z direction (V_1 and V_3, V_2 and V_4 on Figure 2) exhibit identical density of states. Consequently, the orbital ordering appears to be of C-type. When allowing the electronic structure to distort, several changes appear in the orbital occupations. Consecutive atoms along the z direction now prefer to occupy either more of the d_{xz} or the d_{yz} orbital, which results in a mixed G-type (G-o.o.) plus C-type orbital ordering (C-o.o.). The G-o.o. that appears, despite the absence of the Q_2^- motion, is allowed via the Kugel-Khomskii mechanism [45]. This mixed orbital ordering produces an asymmetry between the VO_2 planes, as indicated by the two magnitudes of magnetic moments in each layer (1.816±0.001 μ_B and 1.819±0.001 μ_B). The mixed orbital ordering also appears in the bulk vanadates, such as the G-o.o.+C-o.o. ground state of $LaVO_3$ or $PrVO_3$ (previously thought to be just G-o.o. from experiments) [25, 26]. However, here it is not enough to break the inversion symmetry along the z axis yielding no out-of-plane polarization. The second necessary ingredient is the symmetry breaking due to the A and A' ordering along the [001] direction in the superlattices. The combination of both effects (in the AO and VO_2 planes) is required to break inversion symmetry along the z axis and to produce the out-of-plane polarization. The result is an orbital ordering induced ferroelectricity in vanadate superlattices.

Interestingly, the direction of the orbital ordering induced ferroelectric polarization is found to be arbitrary, and both +0.04 and -0.04 $\mu C.cm^{-2}$ are observed. Each state displays a reversal of the magnitude of the magnetic moment of the two VO_2 planes. Starting from these two possibilities, we performed the geometry relaxation and it ended with the previously identified Pb ground states, with both possibilities (up and down) for the out-of-plane polarization. We note that the difference in magnetic moment between both VO_2 planes is more pronounced (1.820±0.001 μ_B and 1.828±0.001 μ_B) after the geometry relaxation. Three new lattice distortions develop to reach the Pb phase: P_z, Q_2^- and ϕ_z^-.

To understand the nature of their appearance, we plot in Figure 4 each potential as a function of the distortion

amplitude. All potentials present single wells, more or less shifted through an improper coupling with the electronic instability. This confirms that the electronic instability is the primary order parameter driving the phase transition. Moreover, the Q_2^- motion presents an energy gain of one to two orders of magnitude larger than those of the ϕ_z^- motion, indicating that the Q_2^- couples more strongly with the electronic instability, which might be expected. Consequently, once the electronic instability condenses, the Q_2^- lattice distortion is forced into the system which consequently produces the lattice part of the polarization through the structural hybrid improper coupling. This Jahn-Teller induced ferroelectricity amplifies by one order of magnitude the electronic out-of-plane polarization. The sign of the three lattice distortions is again imposed by the initial sign (up or down) of the electronic polarization. Consequently, the reversal of P_z through an application of an external electric field would require the reversal of both Q_2^-, ϕ_z^- and the magnitude of the magnetic moment of both VO_2 planes. The saddle point at the midway of this reversal (all three modes equal zero, i.e. the $Pb2_1m$ phase) is of the order of 10 meV higher in energy, which represents a reasonable estimate of the ferroelectric switching barrier. Compared to the rotationally driven ferroelectricity P_{xy}, whose energy barrier is of the order of 0.1 to 1 eV [12, 14, 15], this Jahn-Teller induced ferroelectricity is therefore very likely to be switchable. The large difference between the two energy barriers is due to two different energy landscapes involving i) the robust AFD motions inducing P_{xy} and ii) the relatively soft distortions inducing P_z.

Finally we discuss a novel route to create the technologically desired electrical control of magnetization. Starting from a $Pb2_1m$ phase with an G-AFM magnetic ordering, the application of an external electric field $\vec{E}$ along z will induce P_z in the system through the dielectric effect. As a result, the Q_2^- distortion is automatically induced through the $Q_2^+ Q_2^- P_z$ trilinear term. This electric field induced Q_2^- distortion is a general result for any $(ABO_3)_1/(A'BO_3)_1$ superlattice consisting of two $Pbnm$ perovskites. Since Q_2^- distortions are intimately connected to the G-o.o. and the C-AFM magnetic ordering, for a finite value of $\vec{E}$, the system may switch from the initial G-AFM phase to the C-AFM phase. In reality, the C-AFM phase should exhibit a net weak magnetization from a non collinear magnetic structure as observed in several bulk vanadates of $P2_1/b$ symmetry [28, 30, 53]. Therefore, the application of an electric field may not only switch between AFM orderings, but also produce a net magnetic moment in the material. However, for illustrative purposes, even at the collinear level in our calculations, we can look at the relative stability between the two magnetic states under an external electric field in the YLVO superlattice, which presents the desired $Pb2_1m$ ground state (8 meV lower than the Pb phase).

Figure 5 (top panel) plots the internal energy $U(D)$ of the Pb and $Pb2_1m$ phases as a function of the amplitude of the electric displacement field D applied along the z axis. In such a graph, the switching E-field at which the the Pb phase with the G-o.o./C-AFM ordering becomes more stable than the $Pb2_1m$ phase with the C-o.o./G-AFM ordering, is given by the slope of the common tangent between the two curves and is evaluated to be around 6.54 MV.cm^{-1}. This corresponds to a voltage of 0.50 V for one bilayer (c$\simeq$7.8 Å). This critical electric field could be further decreased by reducing the energy difference between the two phases at zero field. This can be achieved by changing the A cations or applying biaxial epitaxial strain (see supplementary material).

As illustrated in Figure 5, what we demonstrate more generally in the present study is an electric field control of the JT distortions, mediated by their coupling with the polar mode. Since this mechanism arises from universal symmetry relations, we can expect this effect to also appear in other perovskite superlattices, such as nickelates, fluorites or manganites to name a few. This effect may find applications outside the field of magnetoelectrics such as for tunable band gaps and metal-insulator transitions, since the JT distortion affects the electronic structure in general.

CONCLUSIONS

In conclusion, we have identified novel lattice mode couplings in the vanadates, helping to clarify the origin of the unusual coexisting Jahn-Teller phase, and indeed the role of Jahn-Teller distortions in perovskites in general. These findings have enabled the prediction of a novel paradigm for the elusive magnetoelectric multiferroics, based on a Jahn-Teller / orbital ordering induced ferroelectricity. Due to the intimate connection between Jahn-Tellers and orbital ordering with magnetism, this unprecedented type of improper ferroelectric facilitates an electric field control of both orbital-ordering and magnetization. The rationale is completely general, and a challenge for applications will be to identify new materials with a magnetic and co-existing Jahn-Teller phase at room temperature. The demonstration of an electric field control of Jahn-Teller distortions may find more general applications for novel functional devices, outside the field of multiferroics. We hope these discoveries will help motivate future studies that will further unlock the potential of vanadate perovskites, and other Jahn-Teller systems, such as fluorites, nickelates and manganites.
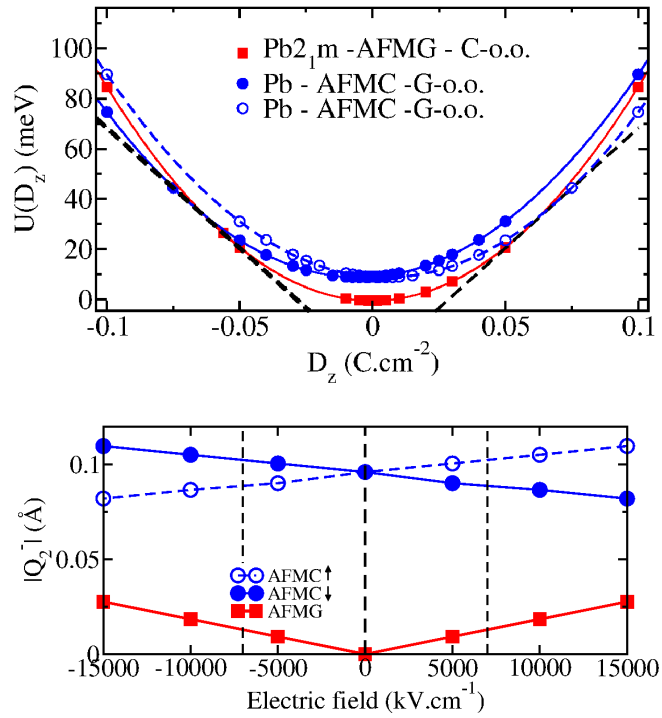
FIG. 5. (top) Internal energy U(D) (in meV) as a function of the electric displacement field D along the z axis for the different phases of YLVO superlattices. The black dashed line is the common tangent of the two potentials defining the value of the switching electric field. Two polar states are possible for the Pb phase starting from an initial up or down P_z polarization. (bottom) Amplitude of Q_2^- distortion as a function of the electric field along the z direction in the $Pb2_1m$-G-AFM phase (red filled squares) and in the Pb-C-AFM phases with initial up (blue open circles) and down (blue filled circles) polarisation in zero field.

METHODS

The basic mechanism we propose here is solely based on symmetry arguments. Symmetry mode analysis of experimental data were performed using amplimodes [47, 48]. The free energy expansion of Equations (1), (2) and (3) is performed using the invariants software from the isotropy code [58]. The results from these symmetry considerations are not dependent on the technical parameters of the first-principles calculations. The latter are only there to illustrate on a concrete basis and quantify the effect. First principles density functional theory calculations were performed using the VASP package [59, 60]. We used a $6 \times 6 \times 4$ Monkhorst-Pack k-point mesh to model the $Pbnm$ $(P2_1/b)$ phase and a plane wave cut off of 500 eV. Optimized Projector Augmented wave (PAW) potentials for PBEsol exchange-correlation functional were used in the calculations. The polarization was computed using the Berry phase approach as implemented in VASP. The study was performed within the LDA+U framework [61, 62]. The LDA+U framework has already been shown to be sufficient to reproduce the ground state of vanadates [37, 63]. The U parameter was first fitted on bulk compounds in order to correctly reproduce the ground state of the bulk vanadates. A value of U=3.5 eV was obtained (see Table 2 and Table 3 in the supporting information). Phonon calculations were performed using the density functional perturbation theory. We used a collinear approach to model the magnetic structures. Structural relaxations were performed until the maximum forces were below 5 μeV.Å^{-1} and the energy difference between conjugate gradient steps was less than 10^{-9} eV. The superlattices were relaxed starting from four different initial guesses: two magnetic orderings (C-AFM and G-AFM) and two space groups ($Pb2_1m$ and Pb, subgroups of $Pbnm$ and $P2_1/b$ respectively for the layered structures). Lattice distortion potentials were plotted as a function of the fractional amplitude of each mode separately appearing in the ground state. In order to determine the electric field required to switch from the $Pb2_1m$ to the Pb phase, the internal energy at fixed D was estimated for each phase as follows. First, the polar atomic distortion pattern ξ associated to the linear response of the system to an electric field E along z was determined from the knowledge of the phonon frequencies and oscillator strengths. Second, the Kohn-Sham energy well $U_{KS}(\xi)$ in terms of the amplitude of ξ was computed, yielding a model $U_{KS}(P^0)$ restricted to the subspace spanned by ξ using $P^0 = Z^*\xi/\Omega$ where Z^* is the Born effective charge associated to ξ, Ω

the unit cell volume. Third, U(D) was deduced as [64]:

$$U(D) = U_{KS}(P^0) + \frac{\Omega}{2\epsilon_0\epsilon_\infty}(D - P^0)^2 \tag{4}$$

where ϵ_0 is the permittivity of vacuum and ϵ_∞, the optical dielectric constant.

AUTHOR CONTRIBUTIONS

J. Varignon, N. C. Bristowe, E. Bousquet and Ph. Ghosez contributed extensively to the work presented in this paper.

COMPETING FINANCIAL INTERESTS

The authors declare no competing financial interests.

---

† These two authors contributed equally
‡ corresponding author: julien.varignon@ulg.ac.be

[1] Bednorz, J. G., Müller, K. A. Possible high T$_c$ superconductivity in the Ba-La-Cu-O system. *Zeitschrift für Physik B Condensed Matter* **64** 189-193 (1986).
[2] Jin, S. *et al.* Thousandfold change in resistivity in magnetoresistive La-Ca-Mn-O films. *Science* **264**, 413-415 (1994).
[3] Zubko, P., Gariglio, S., Gabay, M., Ghosez, Ph., Triscone, J. M. Interface physics in complex oxide heterostructures. *Annu. Rev. Condens. Matter Phys.* **2**, 141-165 (2011).
[4] Hwang, H. *et al.* Emergent phenomena at oxide interfaces. *Nature Materials* **11**, 103-113 (2012).
[5] Tokura, Y., Nagaosa, N. Orbital physics in transition-metal oxides. *Science* **88**, 462-468 (2000).
[6] Dagotto, E. Complexity in strongly correlated electronic systems. *Science* **309**, 257-262 (2005).
[7] Bibes, M., Barthélémy, A. Towards a magnetoelectric memory. *Nature Materials* **7**, 425-426 (2008).
[8] Scott, J. Applications of modern ferroelectrics. *Science* **315**, 954-959 (2007).
[9] Scott, J. Data storage: Multiferroic memories. *Nature Materials* **6**, 256-257 (2007).
[10] Bousquet, E. *et al.* Improper ferroelectricity in perovskite oxide artificial superlattices. *Nature* **452**, 732-736 (2008) .
[11] Fukushima, T., Stroppa, A., Picozzi, S., Perez-Mato, J. M. Large ferroelectric polarization in the new double perovskite NaLaMnWO$_6$ induced by non-polar instabilities. *Phys. Chem. Chem. Phys.* **13**, 12186-12190 (2011).
[12] Rondinelli, J. M., Fennie, C. J. Octahedral rotation-induced ferroelectricity in cation ordered perovskites. *Adv. Materials* **24**, 1961-1968 (2012).
[13] Benedek, N. A., Fennie, C. J. Hybrid improper ferroelectricity: a mechanism for controllable polarization-magnetization coupling. *Phys. Rev. Lett.* **106**, 107204 (2011).
[14] Zanolli, Z., Wojdel, J. C., Iñiguez, J, Ghosez, Ph. Electric control of the magnetization in BiFeO$_3$/LaFeO$_3$ superlattices. *Phys. Rev. B* **88**, 060102(R) (2013).
[15] Mulder, A. T., Benedek, N. A., Rondinelli, J. M., Fennie, C. J. Turning ABO$_3$ antiferroelectrics into ferroelectrics: Design rules for practical rotation-driven ferroelectricity in double perovskites and A$_3$B$_2$O$_7$ ruddlesden-popper compounds. *Adv. Func. Mater.* **23**, 4810-4820 (2013).
[16] Bellaiche, L., Íñiguez, J. Universal collaborative couplings between oxygen-octahedral rotations and antiferroelectric distortions in perovskites. *Phys. Rev. B* **88**, 014104 (2013).
[17] Yang, Y, Íñiguez, J., Mao, A.-J., Bellaiche, L. Prediction of a Novel Magnetoelectric Switching Mechanism in Multiferroics. *Phys. Rev. Lett.* **112**, 057202 (2014).
[18] Stroppa, A., Barone, P., Jain, P., Perez-Mato, J. M., Picozzi, S. Hybrid improper ferroelectricity in a multiferroic and magnetoelectric metal-organic framework. *Adv. Mater.* **25**, 2284-2290 (2013).
[19] Tian, Y. *et al.* High-temperature ferroelectricity and strong magnetoelectric effects in a hybrid organic-inorganic perovskite framework. *Phys. Status Solidi RRL* **1**, 1-6 (2014). .

[20] Bersucker, I. *et al.* The Jahn-Teller Effect: Fundamentals and Implications for Physics and Chemistry, Vol. 97 (eds. Köppel, H., Yarkony, D. R., Barentzen, H.) (Springer, 2009).

[21] Onoda, M., Ohta, H., Nagasawa, H. Metallic properties of perovskite oxide SrVO$_3$. *Solid State Comm.* **79**, 281-285 (1991).

[22] Wold, A., Ward, R. Perovskite-type oxides of cobalt, chromium and vanadium with some rare earth elements. *J. Am. Chem. Soc.* **76**, 1029-1030 (1954).

[23] Bordet, P. *et al.* Structural aspects of the crystallographic-magnetic transition in LaVO$_3$ around 140 K. *J. Solid State Chem.* **106**, 253-270 (1993).

[24] Kawano, H., Yoshizawa, H., Ueda, Y. Magnetic behavior of a mott-insulator YVO$_3$. *J. Phys. Soc. Jpn* **63**, 2857-2861 (1994).

[25] Miyasaka, S., Okimoto, S., Iwama, N., Tokura, Y. Spin-orbital phase diagram of perovskite-type RVO$_3$ (R= Rare-Earth ion or Y). *Phys. Rev. B* **68**, 100406 (2003).

[26] Sage, M. H., Blake, G., Marquina, C., Palstra, T. Competing orbital ordering in RVO$_3$ compounds: High-resolution X-ray diffraction and thermal expansion. *Phys. Rev. B* **76**, 195102 (2007).

[27] Mahajan, A., Johnston, D., Torgeson, D., Borsa, F. Magnetic properties of LaVO$_3$. *Phys. Rev. B* **46**, 10966 (1992).

[28] Ren, Y. *et al.* Temperature-induced magnetization reversal in a YVO$_3$ single crystal. *Nature* **396**, 441-444 (1998).

[29] Tung, L. *et al.* Spin, orbital ordering, and magnetic dynamics of LaVO$_3$: Magnetization, heat capacity, and neutron scattering studies. *Phys. Rev. B* **78**, 054416 (2008).

[30] Tung, L., Lees, M., Balakrishnan, G., Paul, D. M. Magnetization reversal in orthovanadate RVO$_3$ compounds (R= La, Nd, Sm, Gd, Er, and Y): Inhomogeneities caused by defects in the orbital sector of quasi-one-dimensional orbital systems. *Phys. Rev. B* **75**, 104404 (2007).

[31] Ulrich, C. *et al.* Magnetic neutron scattering study of YVO$_3$: Evidence for an orbital peierls state. *Phys. Rev. Lett.* **91**, 257202 (2003).

[32] Arima, T. H., Tokura, Y. Optical study of electronic structure in perovskite-type RMO$_3$ (R= La, Y; M= Sc, Ti, V, Cr, Mn, Fe, Co, Ni, Cu). *J. Phys. Soc. Jpn* **64**, 2488-2501 (1995).

[33] Noguchi, M. *et al* Synchrotron X-ray-diffraction study of orbital ordering in YVO$_3$. *Phys. Rev. B* **62**, R9271 (2000).

[34] Khaliullin, G., Horsch, P., Oleś, A. M. Spin order due to orbital fluctuations: Cubic vanadates. *Phys. Rev. Lett.* **86**, 3879 (2001).

[35] Sawada, H., Terakura, K. Orbital and magnetic orderings in localized t_{2g} systems, YTiO$_3$ and YVO$_3$: Comparison with a more itinerant e_g LaMnO$_3$. *Phys. Rev. B* **58**, 6831 (1998).

[36] Blake, G. R., Palstra, T., Ren, Y., Nugroho, A. A., Menovsky, A. Transition between orbital orderings in YVO$_3$. *Phys. Rev. Lett.* **87**, 245501 (2001) .

[37] De Raychaudhury, M., Pavarini, E., Andersen, O. Orbital fluctuations in the different phases of LaVO$_3$ and YVO$_3$. *Phys. Rev. Lett.* **99**, 126402 (2007).

[38] Carpenter, M. A., Howard, C. J. Symmetry rules and strain/order-parameter relationships for coupling between octahedral tilting and cooperative Jahn-Teller transitions in ABX$_3$ perovskites. i. theory. *Acta Cryst. B* **65**, 134-146 (2009).

[39] Carpenter, M. A., Howard, C. J. Symmetry rules and strain/order-parameter relationships for coupling between octahedral tilting and cooperative Jahn-Teller transitions in ABX$_3$ perovskites. i. application. *Acta Cryst. B* **65**, 147-159 (2009).

[40] Varignon, J., Bristowe, N. C., Ghosez, P. Electric field control of Jahn-Teller distortions in bulk perovskites. arXiv:1505.03413.

[41] Miao, N., Bristowe, N. C., Xu, B., Verstraete, M. J., Ghosez, Ph. First-principles study of the lattice dynamical properties of strontium ruthenate. *J. Phys.: Condens. Matter* **26**, 035401 (2014).

[42] Goodenough, J. B. Jahn-Teller phenomena in solids. *Annual. Rev. of Materials Science* **28**, 1-27 (1998).

[43] Goodenough, J. B. An interpretation of the magnetic properties of the perovskite-type mixed crystals La$_{1-x}$Sr$_x$CoO$_{3-\lambda}$. *J. Phys. Chem. Solids* **6**, 287-297 (1958).

[44] Kanamori, J. Superexchange interaction and symmetry properties of electron orbitals. *J. Phys. Chem. Solids* **10**, 87-98 (1959).

[45] Kugel, K., Khomskii, D. Crystal-structure and magnetic properties of substances with orbital degeneracy. *Zh. Eksp. Teor. Fiz* **64**, 1429-1439 (1973).

[46] Sage, M. H., Blake, G. R., Nieuwenhuys, G. J., Palstra, T. T. M. Evidence for Electronic Phase Separation between Orbital Orderings in SmVO$_3$. *Phys. Rev. Lett.* **96**, 036401 (2006).

[47] Orobengoa, D., Capillas, C., Aroyo, M. I., Perez-Mato; J. M. Amplimodes: symmetry-mode analysis on the bilbao crystallographic server. *J. App. Cryst.* **42**, 820-833 (2009).

[48] Perez-Mato, J. M., Orobengoa, D., Aroyo, M. Mode crystallography of distorted structures. *Acta Cryst. Section A* **66**, 558-590 (2010).

[49] Reehuis, M. *et al.* Neutron diffraction study of YVO$_3$, NdVO$_3$, and TbVO$_3$. *Phys. Rev. B* **73**, 094440 (2006).

[50] Seim, H., Fjellvag, H. Non-stoichiometric LaVO$_3$. i. synthesis and physical properties. *Acta Chem. Scand.* **52**, 1096-1103 (1998).

[51] Glazer, A. The classification of tilted octahedra in perovskites. *Acta Cryst. B.* **28**, 3384-3392 (1972).

[52] Goldschmidt, V. M. Die gesetze der krystallochemie. *Naturwissenschaften* **14**, 477-485 (1926).

[53] Zhang, Q. *et al.* Impact of the various spin-and orbital-ordering processes on the multiferroic properties of orthovanadate DyVO$_3$. *Phys. Rev. B* **90**, 024418 (2014).

[54] Varignon, J., Bristowe, N. C., Bousquet, E., Ghosez, Ph. Novel magneto-electric multiferroics from first-principles. *Comptes Rendus Physique* **16**, 153-167 (2015).

[55] Ghosez, Ph., Triscone, J. M. Multiferroics: Coupling of three lattice instabilities. *Nature Materials* **10**, 269-270 (2011).

Mode (Irreps)	YVO$_3$			PrVO$_3$		LaVO$_3$	
	Pbnm	P2$_1$/b	Pbnm	Pbnm	P2$_1$/b	Pbnm	P2$_1$/b
	295K [49]	100K [36]	5K [49]	295K [26]	5K [26]	298K [50]	10K [23]
$\phi_{xy}^-+\phi_z^-$ (R$_5^-$)	-	1.72	-	-	1.34	-	1.16
ϕ_{xy}^- (R$_5^-$)	1.71	-	1.73	1.34	-	1.17	-
ϕ_z^+ (M$_2^+$)	1.22	1.24	1.22	0.94	0.96	0.68	0.75
Q$_2^+$ (M$_3^+$)	0.05	0.06	0.14	0.02	0.02	0.08	0.01
Q$_2^-$ (R$_3^-$)	-	0.10	-	-	0.18	-	0.08
X$_5^-$ (X$_5^-$)	0.86	0.87	0.87	0.53	0.64	0.37	0.39
X$_3^-$ (X$_3^-$)	-	0.01	-	-	0.06	-	0.00

TABLE I. Amplitudes of distortions (in Å) on experimental structures of vanadates at different temperatures. In the $P2_1/b$ symmetry, both ϕ_{xy}^- and ϕ_z^- AFD motions belong to the same irreducible representation (R$_5^-$ mode) even if the ϕ_z^- amplitude is likely very small. The reference structure was chosen as a cubic structure whose lattice vector corresponds to the pseudo cubic lattice vector associated to the room temperature $Pbnm$ phase.

[56] Saha-Dasgupta, T. Ferroic properties in bi-component perovskites: artificial superlattices and naturally forming compounds. *J. Phys. Condens. Matter* **26**, 193201 (2014).

[57] Benedek, N. A., Rondinelli, J. M., Djani, H., Ghosez, Ph. Lightfoot, P. Understanding ferroelectricity in layered perovskites: new ideas and insights from theory and experiments. *Dalton Transactions* **23**, 10543-10558 (2015).

[58] Hatch, D. M., Stokes, H. T. Invariants: program for obtaining a list of invariant polynomials of the order-parameter components associated with irreducible representations of a space group. *J. App. Cryst.* **36**, 951-952 (2003).

[59] Kresse, G., Haffner, J. Ab initio molecular dynamics for liquid metals, Phys. Rev. B 47 (1993) 558.

[60] Kresse, G., Furthmüller, J. Efficiency of ab-initio total energy calculations for metals and semiconductors using a plane-wave basis set. *Comp. Mat. Science* **6**, 15-50 (1996).

[61] Anisimov, V. I., Zaanen, J., Andersen, O. K. Band theory and Mott insulators: Hubbard U instead of stoner I. *Phys. Rev. B* **44**, 943 (1991).

[62] Liechtenstein, A. I., Anisimov, V. I., Zaanen, J. Density-functional theory and strong interactions: Orbital ordering in Mott-Hubbard insulators. *Phys. Rev. B* **52**, R5467 (1995) .

[63] Fang, Z., Nagaosa, N. Quantum versus jahn-teller orbital physics in YVO$_3$ and LaVO$_3$. *Phys. Rev. Lett.* **93**, 176404 (2004).

[64] Stengel, M., Vanderbilt D., Spaldin, N. A. First-principles modeling of ferroelectric capacitors *via* constrained displacement field calculations. *Phys. Rev. B* **80**, 224110 (2009).

Coupling and electrical control of structural, orbital and magnetic orders in perovskites - Supplementary material

Julien Varignon[a],[1],[†] Nicholas C. Bristowe,[1],[2],[†] Eric Bousquet,[1] and Philippe Ghosez[1]

[1]*Physique Théorique des Matériaux, Université de Liège (B5), B-4000 Liège, Belgium*[‡]

[2]*Department of Materials, Imperial College London, London SW7 2AZ, UK*

(Dated: February 20, 2015)

[a] corresponding author: julien.varignon@ulg.ac.be
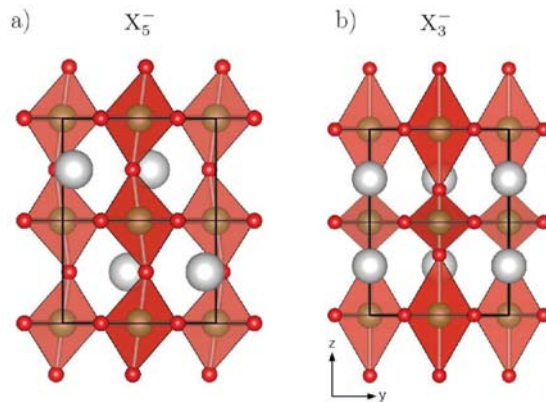
ADDITIONAL LATTICE DISTORTIONS

FIG. 1. Additional antipolar motions appearing in the bulk ground states. a) X_5^- anti polar mode appearing in both *Pbnm* and $P2_1/b$ phases. b) X_3^- antipolar mode appearing exclusively in the $P2_1/b$ phase.

OPTIMIZED BULK VANADATES AT 0K

In order to extract the effective U parameter for our DFT calculations, we fitted its value on bulk vanadates in order to correctly reproduce the ground state of YVO$_3$, PrVO$_3$ and LaVO$_3$. With an effective parameter of U of 3.5 eV, we correctly reproduce the *Pbnm* ground state of YVO$_3$ and the $P2_1/b$ ground state of both PrVO$_3$ and LaVO$_3$. Optimized lattice parameters and symmetry mode analysis are given in Tables I and II respectively. Within our DFT calculations, YVO$_3$ exhibits a gap of 1.95 eV in close comparison with experimental value (around 1.6 eV) [1], while LaVO$_3$ and PrVO$_3$ develop band gaps of 1.70 eV and 1.93 eV respectively, slightly overestimated [2].

OPTIMIZED (AVO$_3$)$_1$/(A'VO$_3$)$_1$ LAYERED STRUCTURES

Symmetry mode analysis

Symmetry mode analysis of our optimized vanadate layered structures are provided in Table III. The superlattice is insulating and develops a band gap of 1.86 eV.

Origin of P$_{xy}$

As discussed in the main paper, bulk vanadates develop a *Pbnm* symmetry at room temperature and hence the layered structures should present the equivalent $Pb2_1m$ symmetry. In the $Pb2_1m$ phase, four main distortions are present: ϕ_{xy}^-, ϕ_z^+, Q_2^+ and P$_{xy}$. In order to understand the driving force leading to this metastable $Pb2_1m$ symmetry, we added some amplitude of distortions leading to this symmetry in a hypothetical $P4/mmm$ phase. Potentials are plotted in Figure2. As expected, the two AFD motions present double wells and are strongly unstable (energy gains around 1 eV) while P$_{xy}$ and Q_2^+ are stable. Consequently, ϕ_{xy}^- and ϕ_z^+ are the primary order parameters leading to the $Pb2_1m$ symmetry, and P$_{xy}$ and Q_2^+ appear through improper couplings. These potentials confirm the hybrid improper character of the in-plane P$_{xy}$ polarization [6–8].
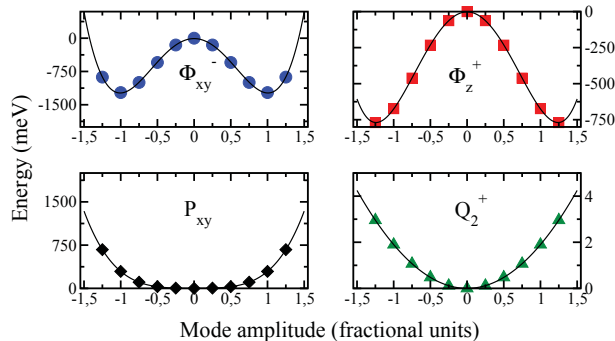
FIG. 2. Energy gains (in meV) by condensing several amplitudes of distortions leading to the $Pb2_1m$ (AFMG) within the P_4/mmm structure.

STRAIN EFFECT ON $(AVO_3)_1/(A'VO_3)_1$ LAYERED STRUCTURES

For potential applications, the proposed superlattices can be grown on given substrates. The pseudocubic parameters (defined as the mean value of the low symmetry lattice parameters) are 3.88 Å, 3.88 Å and 3.92 Å for YLVO and PLVO superlattices respectively. We chose cubic SrTiO$_3$ (3.905 Å) and KTaO$_3$ (3.9885 Å) as two potential substrates and performed a geometry relaxation of the two superlattices constraining both in-plane pseudocubic lattice parameters to those of the substrates [9]. Results are displayed in Table IV. The effect of the substrates is to tune the relative energy difference between the two magnetic orderings, and hence between the two orbital-ordered phases. A SrTiO$_3$ substrate seems to favor an AFMG magnetic ordering, and consequently a pure Q_2^+ phase. On the contrary, going to a KTaO$_3$ substrate applies a moderate tensile strain and favors an AFMC magnetic ordering for the two superlattices. These strain effects then open the way to an indirect control of the magnetism and the orbital ordering playing with the strain imposed by the substrates. Indeed, growing $(AVO_3)_1/(A'VO_3)_1$ layered structures on a piezoelectric substrates, an indirect coupling with the electric field may appear:

$$\text{coupling} \propto \frac{electric}{strain} \times \frac{strain}{magnetism}$$

Applying an external field on the substrate induces a strain on the vanadate layered structure, and consequently this latter can switch both magnetic and orbital orderings.

[†] These two authors contributed equally

[‡] julien.varignon@ulg.ac.be

[1] Tsvetkov, A. *et al.* Structural, electronic, and magneto-optical properties of YVO$_3$. *Phys. Rev. B* **69**, 075110 (2004).

[2] Arima, T., Tokura, Y., Torrance, J. Variation of optical gaps in perovskite-type 3d transition-metal oxides. *Phys. Rev. B* **48**, 17006 (1993).

[3] Reehuis, M. *et al.* Neutron diffraction study of YVO$_3$, NdVO$_3$, and TbVO$_3$. *Phys. Rev. B* **73**, 094440 (2006).

[4] Sage, M., Blake, G., Marquina, C., Palstra, T. Competing orbital ordering in RVO$_3$ compounds: High-resolution X-ray diffraction and thermal expansion. *Phys. Rev. B* **76**, 195102 (2007).

[5] Bordet, P. *et al.* Structural aspects of the crystallographic-magnetic transition in LaVO$_3$ around 140 K. *J. Solid State Chem.* **106**, 253-270 (1993).

[6] Bousquet, E. *et al.* Improper ferroelectricity in perovskite oxide artificial superlattices. *Nature* **452**, 732-736 (2008).

[7] Rondinelli, J. M., Fennie, C. J. Octahedral rotation-induced ferroelectricity in cation ordered perovskites. *Adv. Materials* **24**, 1961-1968 (2012).

[8] Fukushima, T., Stroppa, A., Picozzi, S., Perez-Mato, J. M. Large ferroelectric polarization in the new double perovskite NaLaMnWO$_6$ induced by non-polar instabilities. *Phys. Chem. Chem. Phys.* **13**, 12186-12190 (2011).

[9] Schlom, D. G. *et al.* Strain tuning of ferroelectric thin films. *Annu. Rev. Mater. Res.* **37**, 589-626 (2007).

		YVO$_3$		PrVO$_3$	LaVO$_3$
		$Pbnm$ AFMG	$P2_1/b$ AFMC	$P2_1/b$ AFMC	$P2_1/b$ AFMC
a(Å)	th.	5.28	5.27	5.48	5.55
	exp.	5.29(5K) [3]	5.28(85K) [3]	5.48(5K) [4]	5.56(10K) [5]
b (Å)	th.	5.61	5.65	5.68	5.64
	exp.	5.59(5K) [3]	5.62(85K) [3]	5.61(5K) [4]	5.59(10K) [5]
c (Å)	th.	7.58	7.55	7.72	7.76
	exp.	7.56(5K) [3]	7.54(85K) [3]	7.69(5K) [4]	7.75(10K) [5]
α (°)	th.	-	90.03	90.14	90.15
	exp.	-	90.02(85K) [3]	90.15(5K) [4]	90.13(10K) [5]

TABLE I. Optimized lattice parameters for the bulk vanadates at 0 K. Experimental values are given for comparison.

	YVO$_3$	PrVO$_3$	LaVO$_3$
Mode (Irreps)	$Pbnm$	$P2_1/b$	$P2_1/b$	$P2_1/b$
ϕ_{xy}^- $(+\ \phi_z^-)$ (R_5^-)	-	1.81	1.42	1.32
ϕ_{xy}^- (R_5^-)	1.83	-	-	-
ϕ_z^+ (M_2^+)	1.24	1.25	0.97	0.89
Q_2^+ (M_3^+)	0.15	0.06	0.02	0.01
Q_2^- (R_3^-)	-	0.10	0.10	0.09
X_5^- (X_5^-)	0.90	0.90	0.65	0.52
X_3^- (X_3^-)	-	0.05	0.01	0.00

TABLE II. Amplitudes of distortions (in Å) on our optimized bulk vanadates at 0 K with respect to a hypothetical pseudocubic phase. In the $P2_1/b$ symmetry, both ϕ_{xy}^- and ϕ_z^- belong to the same irreps, even if ϕ_z^- amplitude of distortion should remain extremely small.

Mode (Irreps)	YLVO (0K) $Pb2_1m$-AFMG	PLVO (0K) Pb-AFMC
ϕ_{xy}^- (M_5^-)	1.58	1.36
ϕ_z^+ (M_2^+)	1.13	0.94
ϕ_z^- (M_4^-)	-	0.01
M_{JT} (M_3^+)	0.13	0.01
R_{JT} (M_1^-)	-	0.09
P_{xy} (Γ_5^-)	0.76 (7.89 $\mu C.cm^{-2}$)	0.59 (2.94 $\mu C.cm^{-2}$)
P_z (Γ_3^-)	- -	0.00(4) (0.34 $\mu C.cm^{-2}$)

TABLE III. Amplitudes of distortions (in Å) on our optimized bulk vanadates at 0 K with respect to a hypothetical cube on cube phase ($P4/mmm$). In the $P2_1/b$ symmetry, both ϕ_{xy}^- and ϕ_z^- belong to the same irreps, even if ϕ_z^- amplitude of distortion should remain extremely small.

		SrTiO$_3$		Fully relaxed		KTaO$_3$	
		AFMG	AFMC	AFMG	AFMC	AFMG	AFMC
YLVO	ΔE	0	+24	0	+8	0	-10
	c/a	0.98	0.98	1.01	1.01	0.95	0.95
PLVO	ΔE	0	+8	0	-4	0	-13
	c/a	1.00	1.00	1.00	1.00	0.96	0.96

TABLE IV. Amplitudes of distortions (in Å) on our optimized bulk vanadates at 0 K with respect to a hypothetical pseudocubic phase. In the $P2_1/b$ symmetry, both ϕ_{xy}^- and ϕ_z^- belong to the same irreps, even if ϕ_z^- amplitude of distortion should remain extremely small.